# Designing a Novel Trigonal Silicon Material: First-Principles Calculations

Q. Fan[a,b,*], Y. Li[a], R. Yang[a], X. Yu[c] and S. Yun[d]

[a] *College of Information and Control Engineering, Xi'an University of Architecture and Technology, Xi'an 710055, China*
[b] *Shaanxi Key Laboratory of Nano Materials and Technology, Xi'an 710055, China*
[c] *Department of Mechanical and Electrical Engineering, Hetao College, Bayannur, Inner Mongolia 015000, China*
[d] *Functional Materials Laboratory (FML), School of Materials Science and Engineering, Xi'an University of Architecture and Technology, Xi'an 710055, China*

Received: 13.11.2023 & Accepted: 09.02.2024

Doi: 10.12693/APhysPolA.145.273 *e-mail: fanqy@xauat.edu.cn

As the cornerstone of many high-technological things, semiconductor silicon material has been widely studied in the past few decades. The present study introduces a new type of silicon allotrope named tri-$Si_{18}$, belonging to the space group $P3_221$. Based on first-principles calculation, its structure characteristics, stability, electronic properties, and thermal conductivity are systematically investigated and analyzed. The elastic constant and phonon spectrum of tri-$Si_{18}$ demonstrate its mechanics and dynamics stability. The relative enthalpy of tri-$Si_{18}$ is only 0.089 eV/atom, which is more favorable than that of most silicon allotropes. Furthermore, the tri-$Si_{18}$ exhibits elastic anisotropy, particularly in the direction of [100], [010], [110], and [111]. In addition, tri-$Si_{18}$ is a semiconductor material with an indirect band gap of 1.770 eV. More interestingly, the minimum thermal conductivity of tri-$Si_{18}$ reached 1.10 W/(K cm), which is greater than that of $I$-4 Si, $C2/m$-20 Si, $P222_1$ Si, $Amm2$ Si, $Pm$-$3m$ Si, and $Si_{64}$. It is suggested that if tri-$Si_{18}$ is used to make microelectronic devices, they may have better heat dissipation capacity. Due to its lower relative enthalpy and taller minimum thermal conductivity, tri-$Si_{18}$ can be used in a diverse variety of optoelectronic materials and in electronic device fabrication.

topics: silicon, first-principles calculations, indirect band gap, thermal conductivity

## 1. Introduction

Silicon is an extremely common element and the second most abundant material that makes up the crust of the Earth. Due to its unique crystal structure and excellent electronic properties, silicon materials play an important role in our daily life and industrial manufacturing. With the advancement of technology and the rapid growth of the semiconductor industry, the demand for silicon materials in the semiconductor industry has become more intensified, so exploring new homogeneous silicon has become the current research hotspot [1–12], and the emergence of new structures may result in excellent performance.

Most of the chemical and physical properties of silicon have a close relation with its own microscopic crystal structure. Currently, many silicon chains with excellent physical properties have been proposed theoretically to guide future experimental synthesis and ultimately meet the needs of industrial silicon materials [5, 13–15]. For example, Guo et al. [13] introduced a direct semiconductor silicon allotrope $h$-$Si_6$, which has a band gap of 0.61 eV. Furthermore, $h$-$Si_6$ has excellent sun-absorbing performance and electron transfer characteristics. Based on the theory of density function, Fan et al. [14] discovered two Si materials, namely $Cm$-32 silicon and $P21/m$ silicon, which exhibit a direct band gap. These structures demonstrate outstanding photovoltaic capability and can be effectively utilized in the development of thin-film solar cells. Wang et al. [5], through the utilization of *ab initio* calculations under ambient pressure, discovered six metastable forms of silicon with direct or quasi-direct band gaps ranging from 0.39 to 1.25 eV. Moreover, these forms exhibit superior optical properties compared to $Fd$-$3m$ silicon. Amsler et al. [15] conducted a comprehensive investigation of silicon allotropes using a modified *ab initio* minima hopping crystal structure prediction method. They found that compared with traditional diamond-Si, the density of silicon clathrates is low, and the overlap between the absorption spectrum and solar spectrum is stronger, making them very promising for thin-film photovoltaic applications.

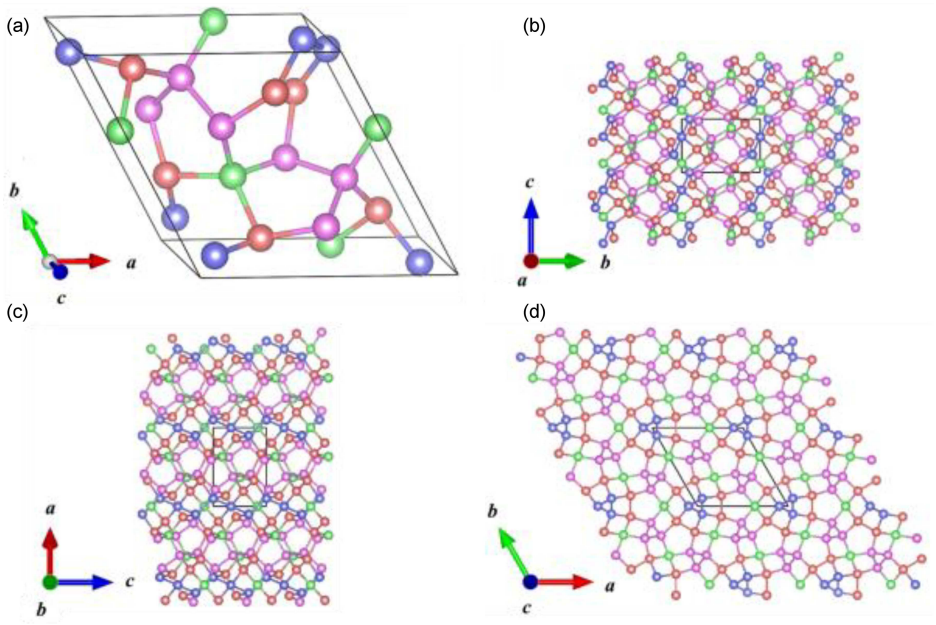


Fig. 1. Crystal structure of tri-$Si_{18}$ in the $P3_221$ phase (a) and the $P3_221$ phase along the $bc$ plane (b), the $ac$ plane (c), and the $ab$ plane (d). There are four unequal atoms, Si1, Si2, Si3, and Si4, represented by orange, purple, blue, and green, respectively.

In this study, we constructed a novel silicon allotrope tri-$Si_{18}$ by resorting to the random sampling strategy combined with space group and graph theory ($RG^2$ [16, 17]) and calculated its physical properties by first-principles calculations. In the light of first-principles calculations, calculation materials have contributed to tremendous achievements in material design and performance prediction [18–24]. The space group of the crystal structure of tri-$Si_{18}$ is $P3_221$, which belongs to the trigonal crystal system. In addition, the mechanical and electronic properties, stability, and minimum thermal conductivity of tri-$Si_{18}$ were thoroughly investigated. Tri-$Si_{18}$ is an indirect band gap semiconductor material. The minimum thermal conductivity coefficient of tri-$Si_{18}$ is similar to that of diamond-Si, so tri-$Si_{18}$ is anticipated to play a significant role in thermoelectric materials.

## 2. Calculation methods

All theoretical calculations are rooted in first-principles calculations in density generalized function theory (DFT) [25, 26] implemented by MedeA-VASP [27, 28]. The exchange–correlation generalization is performed by the generalized gradient approximation (GGA), and this calculation was proposed by Perdew, Burke, and Ernzerhof (PBE) [29]. A 340 eV threshold is employed as the cutoff energy for the plane wave simulations. The core electron interactions were geometrically optimized using ultrasoft pseudopotentials [30], and the structural parameters were calculated by applying the Broyden–Fletcher–Goldfarb–Shanno (BFGS) algorithm [31]. The Monkhorst–Pack scheme [32] is implemented to sample at $5 \times 5 \times 8$ $k$-points in the Brillion zone. The elastic constants were computed utilizing the strain–stress method. Using the Voigt–Reuss–Hill (VRH) [33] method, the bulk modulus ($B$) and shear modulus ($G$) are calculated. The electronic energy band structure was determined utilizing the Heyd–Scuseria–Ernzerhof (HSE06) [34, 35] hybrid general function. In order to study the dynamical stability of the acquired structures, the phonon spectrum of tri-$Si_{18}$ was obtained through the implementation of density functional perturbation theory (DFPT) [36].

## 3. Results and discussion

The space group of tri-$Si_{18}$ is $P3_221$ (No. 154), which belongs to the trigonal crystal system. It can be clearly observed in Fig. 1a that there are four unequal atoms, Si1, Si2, Si3, and Si4, in the structure of tri-$Si_{18}$, which are represented by orange, purple, blue, and green, respectively. Each unit cell of tri-$Si_{18}$ has 18 silicon atoms occupying four different Wyckoff positions: Si1 6$c$ (0.80601, 0.67101, 0.09972), Si2 6$c$ (0.78624, 0.37632, −0.62794), Si3 3$a$ (0.90052, 0.00000, 0.66667), Si4 3$b$ (0.63193, 0.00000, 0.16667). The crystal structure of tri-$Si_{18}$ is made up of several consistent five-membered rings and six-membered rings.

The five-membered ring consists of three Si2 atoms, one Si1 atom, and one Si4 atom, and the six-membered ring is made up of two Si1 atoms, two Si2 atoms, one Si3 atom, and one Si4 atom.

TABLE I

The obtained lattice constants $a$ and $c$ [Å], cell volume $V$ [Å$^3$/atom], and density $\rho$ [g/cm$^3$] of tri-Si$_{18}$, Si$_{64}$, and diamond-Si.

| | Method | $a$ | $c$ | $V$ | $\rho$ |
|---|---|---|---|---|---|
| Si$_{18}$ | GGA | 9.055 | 5.315 | 20.970 | 2.224 |
| | LDA | 8.895 | 5.203 | 19.805 | 2.355 |
| Si$_{64}$ | GGA[a] | 10.952 | 14.970 | | 1.662 |
| | LDA[a] | 10.762 | 14.750 | | 1.748 |
| $P2/m$ Si | GGA[b] | 7.253 | 6.294 | | |
| | LDA[b] | 7.136 | 6.187 | | |
| $P222_1$ Si | GGA[b] | 7.495 | 5.410 | | |
| | LDA[b] | 7.345 | 5.258 | | |
| $Cm$-32 Si | GGA[c] | 8.857 | 14.008 | | |
| | LDA[c] | 8.714 | 13.782 | | |
| diamond-Si | GGA | 5.426 | | | |
| | LDA | 5.374 | | | |
| | GGA[d] | 5.465 | | 40.061 | 2.285 |
| | LDA[e] | 5.374 | | | |
| | exper.[f] | 5.431 | | | |

[a]Ref. [37], [b]Ref. [6], [c]Ref. [14], [d]Ref. [38], [e]Ref. [6], [f]Ref. [39].

Table I lists the lattice constants, unit volume, and density of tri-Si$_{18}$, Si$_{64}$, and diamond-Si. The lattice parameters of tri-Si$_{18}$ are calculated as $a = 9.055$ Å and $c = 5.315$ Å in a conventional cell within the GGA level under environmental pressure. According to the data in Table I (see [6, 14, 37–39]), the lattice parameters of diamond-Si calculated by GGA and LDA are $a = 5.426$ Å and $a = 5.374$ Å, respectively. However, compared with the experimental values ($a = 5.431$ Å), it is noticeable that the lattice parameters of diamond-Si calculated by GGA are similar to the experimental values. In addition, Table I reflects that the density of tri-Si$_{18}$ is 2.224 g/cm$^3$, which is lower than that of diamond-Si (2.285 g/cm$^3$) and greater than that of Si$_{64}$ (1.662 g/cm$^3$).

The stability of the material determines whether it can exist stably at normal temperature and pressure after being synthesized in the future. Therefore, stability is also a very important physical property for the novel silicon allotropes, which are proposed theoretically. Table II (see [37, 40–42]) shows that tri-Si$_{18}$ has six independent elastic constants ($C_{11} = 148$, $C_{12} = 47$, $C_{13} = 52$, $C_{14} = -0.03$, $C_{33} = 182$, $C_{44} = 72$, $C_{66} = 50$). The elastic constants are closely related to their mechanical stability and therefore need to satisfy the equation for mechanical stability as follows [43]

$$\begin{aligned} &C_{11} > |C_{12}|, \quad C_{44} > 0, \\ &C_{13}^2 < \tfrac{1}{2}C_{33}(C_{11} + C_{12}), \\ &C_{14}^2 < \tfrac{1}{2}C_{44}(C_{11} - C_{12}) \equiv C_{44}C_{66}. \end{aligned} \tag{1}$$

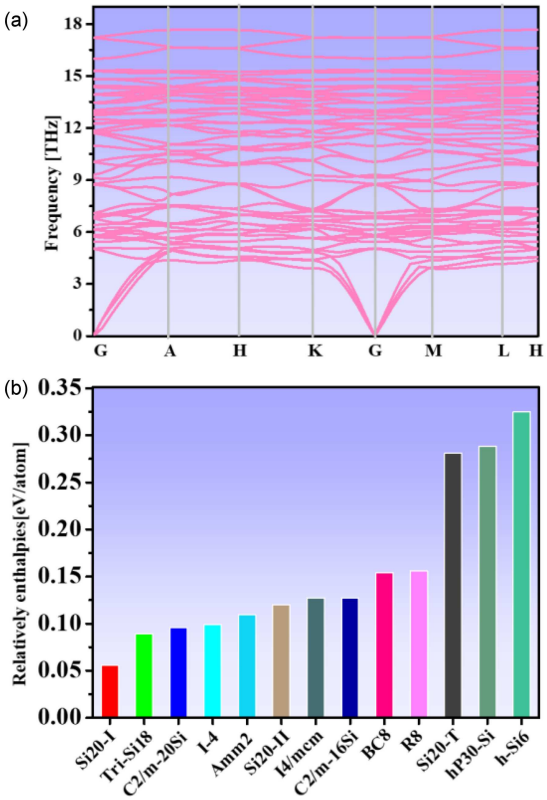


Fig. 2. (a) Phonon spectrum of tri-Si$_{18}$, (b) relative enthalpies of Si20-$I$, tri-Si$_{18}$, $C2/m$-20 Si, $I$-4, $Amm2$, Si20-II, $I4/mcm$, $C2/m$-16Si, BC8, R8, Si20-T, $hP30$-Si, and $h$-Si6.

In the above formula, $C_{66} = \frac{1}{2}(C_{11} - C_{12})$. Data in Table I clearly show that the mentioned matrix is a symmetric matrix, so $C_{ij} = C_{ji}$. The elastic constants have confirmed the mechanical stability of tri-Si$_{18}$ under zero pressure, and the phonon spectrum has proven the dynamic stability [44]. The phonon spectrum of tri-Si$_{18}$ under ambient pressure is shown in Fig. 2a. The phonon spectrum of tri-Si$_{18}$ has no negative frequency in the entire Brillouin zone, thereby indicating that tri-Si$_{18}$ has dynamic stability.

Relative enthalpy is another basic factor that determines how excellent the stability of the material is. Therefore, the relative enthalpies of tri-Si$_{18}$ and other silicon allotropes with respect to diamond-Si have been computed and depicted in Fig. 2b. The relative enthalpy of this silicon phase of tri-Si$_{18}$ is calculated by the following equation

$$\Delta H = \frac{H_{\text{novel-phase}}}{n_1} - \frac{H_{\text{diamond-Si}}}{n_2}, \tag{2}$$

where $H_{\text{diamond-Si}}$ is the enthalpy of diamond-Si; $H_{\text{novel-phase}}$ is the enthalpy of tri-Si$_{18}$ and other silicon allotropes; $n_1$ is the number of atoms in the conventional units of silicon allotropes tri-Si$_{18}$; $n_2$ is the number of atoms in diamond-Si. The relative enthalpy of tri-Si$_{18}$ is calculated as 0.089 eV/atom, where the enthalpy of diamond-Si is zero. In Fig. 2b,

TABLE II

The elastic constants $C_{ij}$ [GPa], elastic moduli $B$, $G$, $E$ [GPa], and Poisson's ratio $v$ of tri-$Si_{18}$, $Si_{64}$, and diamond-Si.

| | Method | $C_{11}$ | $C_{12}$ | $C_{13}$ | $C_{14}$ | $C_{33}$ | $C_{44}$ | $C_{66}$ | $B$ | $G$ | $B/G$ | $E$ | $v$ |
|---|---|---|---|---|---|---|---|---|---|---|---|---|---|
| tri-$Si_{18}$ | GGA | 148 | 47 | 52 | −0.03 | 182 | 72 | 50 | 86 | 59 | 1.46 | 146 | 0.22 |
| | LDA | 162 | 59 | 63 | −2 | 140 | 60 | 51 | 92 | 52 | 1.76 | 132 | 0.26 |
| $Si_{64}$ | GGA[a] | 88 | 20 | 30 | | 95 | 27 | 6 | 48 | 21 | 2.29 | 55 | 0.31 |
| *Amm*2 Si | GGA[b] | 161 | 37 | 42 | | 131 | 44 | 51 | 78 | 51 | 1.54 | 126 | 0.23 |
| *I*-4 Si | GGA[b] | 142 | 48 | 50 | | 145 | 57 | 55 | 80 | 48 | 1.68 | 120 | 0.25 |
| *C*2/*m*-16 Si | GGA[b] | 146 | 51 | 47 | | 164 | 48 | 53 | 82 | 51 | 1.61 | 127 | 0.24 |
| *C*2/*m*-20 Si | GGA[b] | 184 | 36 | 46 | | 143 | 55 | 52 | 83 | 55 | 1.51 | 135 | 0.23 |
| diamond-Si | GGA | 154 | 56 | | | | 79 | | 88 | 64 | 1.38 | 155 | 0.21 |
| | LDA | 163 | 58 | | | | 80 | | 93 | 68 | 1.37 | 164 | 0.21 |
| | GGA[c] | 165 | 65 | | | | 87 | | 88 | 64 | 1.38 | 155 | 0.21 |
| | LDA | 163 | 58 | | | | 80 | | 93 | 68 | 1.37 | 164 | 0.21 |
| | exper.[d] | 166 | 64 | | | | 80 | | 102 | | | | |

[a]Ref. [37], [b]Ref. [40], [c]Ref. [41], [d]Ref. [42].

it can be clearly seen that the relative enthalpy of tri-$Si_{18}$ is greater only compared to Si20-I. It can be inferred that the stability of tri-$Si_{18}$ is higher.

To further investigate the material properties of tri-$Si_{18}$, the bulk modulus ($B$), shear modulus ($G$), Young's modulus ($E$), and Poisson's ratio ($v$) of tri-$Si_{18}$ are calculated and shown in Table II. The bulk modulus and shear modulus are vital parameters used to assess the ability of materials to resist deformation and fracture. Hill [45–47] demonstrated that the Voigt bond acts as an upper bound for the true polycrystalline constant, while the Reuss bond serves as a lower bound. The value of the polycrystal coefficient is determined by taking the average of the Voigt and Reuss coefficients, expressed as

$$G = \frac{(G_R + G_V)}{2} \quad \text{and} \quad B = \frac{(B_R + B_V)}{2}, \quad (3)$$

where "$V$" stands for Voigt bond and "$R$" stands for Reuss key. The ratio of bulk modulus and shear modulus is a measure of the ductile and brittle characteristics of a material. If the ratio of $B$ to $G$ exceeds 1.75, the material exhibits ductility. Conversely, if the ratio falls below this threshold, the material will appear brittle. The bulk modulus [48] and shear modulus of tri-$Si_{18}$ are 86 GPa and 59 GPa, respectively, at the GGA level. According to Table II, the $B/G$ value of tri-$Si_{18}$ is 1.46, which is below the threshold of 1.75. This suggests that tri-$Si_{18}$ is prone to brittleness. Additionally, the $B/G$ value of tri-$Si_{18}$ is greater than that of diamond-Si (1.38) and less than that of $Si_{64}$ (2.26). Hence, tri-$Si_{18}$ is more brittle than diamond-Si. Young's modulus [49] is an important factor pertaining to material tensile elasticity, while Poisson's ratio [50] signifies the ability to measure the bonding force between atoms. Young's modulus and Poisson's ratio can be calculated through the utilization of the subsequent formula

$$E = \frac{9BG}{(3B + G)} \quad \text{and} \quad v = \frac{3B - 2G}{2(3B + G)}. \quad (4)$$

Young's modulus $E$ of tri-$Si_{18}$ is remarkably close to that of diamond-Si, with values of 146 Gpa and 155 Gpa, respectively. The Poisson's ratio for tri-$Si_{18}$ in Table II is 0.22, which is less than 0.26, showing that tri-$Si_{18}$ has decent brittleness. As Table II depicts, the Poisson's ratio of tri-$Si_{18}$ closely parallels that of diamond-Si (0.21), which means that its brittleness remarkably resembles that of diamond-Si.

The three-dimensional surface structure is an effective way of portraying the anisotropic behavior of solid elasticity. This structure of the anisotropic structure with Young's modulus deviates from the sphere. For the isotropic system, the three-dimensional orientation correlation is expressed as a sphere, and the degree of deviation from the sphere reflects the content of anisotropy. As the deviation from the spherical shape increases, the anisotropy of the material becomes more pronounced. In order to further analyze the anisotropy of its elasticity, the three-dimensional Young's modulus structure chart and the two-dimensional Young's modulus structure chart of tri-$Si_{18}$ are constructed as shown in Fig. 3. It can be clearly found in Fig. 3a that the three-dimensional graph of Young's modulus of tri-$Si_{18}$ has a certain deviation in shape, and it can be concluded that the structure has anisotropy.

To gain deeper insights into the elastic anisotropy of tri-$Si_{18}$, further investigation is required. The anisotropy of tri-$Si_{18}$ was studied from Poisson's ratio, shear modulus, and Young's modulus. Table III

TABLE III

The values of $E_{max}$, $E_{min}$, $G_{max}$, $G_{min}$, $v_{max}$, and $v_{min}$, and the ratios of $E_{max}/E_{min}$, $G_{max}/G_{min}$, and $v_{max}/v_{min}$ for tri-$Si_{18}$ at the [100], [010], [011], [101], [001], [110], and [111] directions.

| | $E_{max}$ | $E_{min}$ | $E_{max}/E_{min}$ ratio | $G_{max}$ | $G_{min}$ | $G_{max}/G_{min}$ ratio | $v_{max}$ | $v_{min}$ | $v_{max}/v_{min}$ ratio |
|---|---|---|---|---|---|---|---|---|---|
| [100] | 165 | 125 | 1.32 | 72 | 50 | 1.43 | 0.30 | 0.11 | 2.73 |
| [010] | 165 | 125 | 1.32 | 72 | 50 | 1.43 | 0.30 | 0.11 | 2.73 |
| [001] | 125 | 125 | 1.00 | 72 | 50 | 1.43 | 0.24 | 0.22 | 1.09 |
| [011] | 161 | 125 | 1.29 | 72 | 50 | 1.43 | 0.30 | 0.11 | 2.73 |
| [101] | 161 | 125 | 1.29 | 72 | 50 | 1.43 | 0.30 | 0.11 | 2.73 |
| [110] | 165 | 125 | 1.32 | 72 | 50 | 1.43 | 0.30 | 0.11 | 2.73 |
| [111] | 165 | 125 | 1.32 | 72 | 50 | 1.43 | 0.30 | 0.11 | 2.73 |

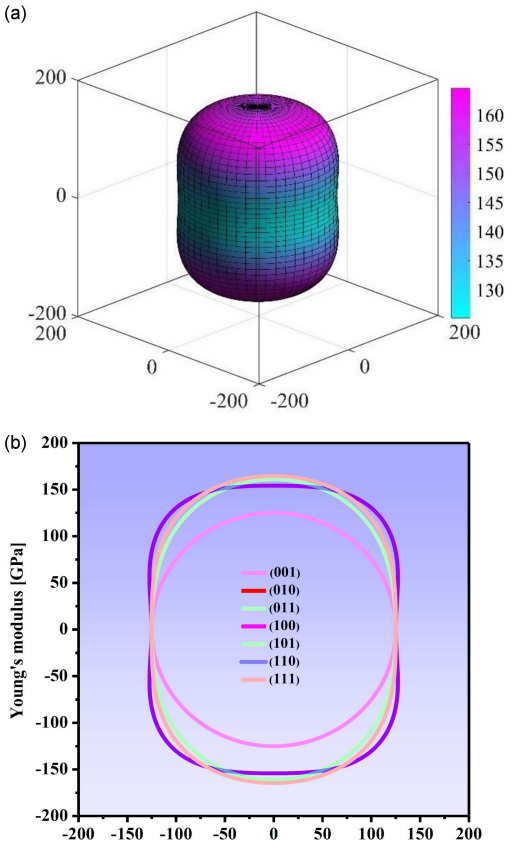


Fig. 3. The directional dependence of Young's modulus (a) and 2D representation of Young's modulus (b) for tri-$Si_{18}$.

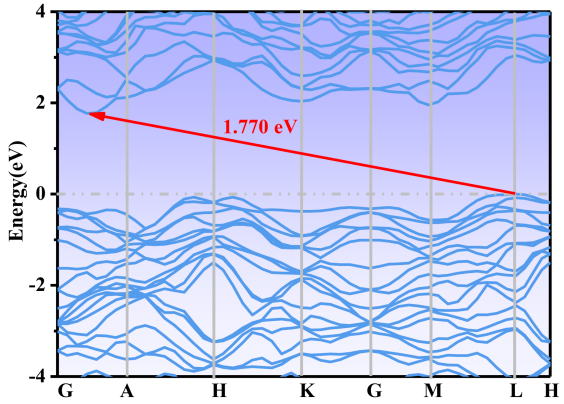


Fig. 4. Electronic band structures of tri-$Si_{18}$.

exhibits the extrema of Young's modulus, shear modulus, and Poisson's ratio, along with the ratio between their maximum and minimum values.

In Table III, the ratio of the maximum value and the minimum value of Young's modulus ($E$) in the [100], [010], [110], and [111] directions is the largest, and its ratio is 1.32, which shows that the highest degree of anisotropy is shown in these specific directions. The ratio of $E_{max}/E_{min}$ in the direction of [011] and [101] is identical, so the anisotropy of Young's modulus ($E$) of tri-$Si_{18}$ is alike in the two directions of [011] and [101]. Especially in the [001] direction, the ratio of $E_{max}/E_{min}$ is 1, which means that this neotype silicon allotrope (tri-$Si_{18}$) behaves isotropically in this direction. The ratio of $G_{max}/G_{min}$ in all directions is the same, which shows that tri-$Si_{18}$ exhibits mechanical anisotropy. In the [001] direction, the ratio between the maximum and minimum values of Poisson's ratio is 1.09, indicating approximately isotropy in this direction.

To better investigate the properties of tri-$Si_{18}$, the electronic band structure chart of tri-$Si_{18}$ is shown in Fig. 4. As is commonly acknowledged, the band gap calculated by PBE is typically undervalued, and the real band gap is generally greater than the calculated result. In order to correct this possible deviation, Heyd et al. [32, 33] put forward an easy-to-control hybrid functional method, resulting in the Heyd–Scuseria–Ernzerhof (HSE06) functional. Therefore, the electronic energy band structure of tri-$Si_{18}$ is calculated using the above-mentioned method. The top of the valence band of tri-$Si_{18}$ is at point L, while the bottom of its conduction band is between points G and A. The coordinates of high-symmetry

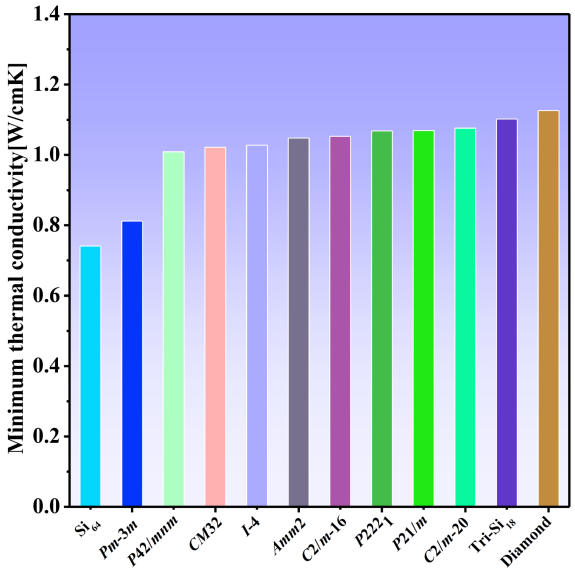


Fig. 5. The minimum thermal conductivities $k_{\min}$ of tri-$Si_{18}$ and other Si allotropes.

points (G, A, H, K, M, L) of tri-$Si_{18}$ are indicated as $(0.000, 0.000, 0.000)$, $(0.000, 0.000, 0.500)$, $(-0.333, 0.667, 0.500)$, $(-0.333, 0.667, 0.000)$, $(0.000, 0.500, 0.000)$, $(0.000, 0.500, 0.500)$, respectively. As a consequence, tri-$Si_{18}$ is a semiconductor with an indirect band gap of 1.770 eV.

Thermal conductivity, also known as the "coefficient of thermal conductivity," quantifies how effective a substance is at conducting heat. Cahill et al. [51, 52] concluded that the connection between the minimum thermal conductivity and temperature and the relational equation can be expressed as

$$\kappa_{\min} = \sqrt[3]{\frac{n^2\pi}{6}} k_{\mathrm{B}} \sum_i v_i \left(\frac{T}{\Theta_i}\right)^2 \int_0^{\Theta_i/T} \frac{\mathrm{d}x\, x^3 \mathrm{e}^x}{(\mathrm{e}^x - 1)^2}, \tag{5}$$

where $n$ represents the atomic number density, $k_{\mathrm{B}}$ stands for the Boltzmann constant, and $T$ stands for the temperature. The sum consists of three sound wave velocities of $v_i$, i.e., two shear sound wave speeds $v_s$ ($v_s = (B_H + \frac{4}{3}G_H)/\rho$), and one compressed sound wave speed $v_p = \sqrt{G_H/\rho}$. The cutoff frequency $\Theta_i$ for each polarization is expressed in K and is given as

$$\Theta_i = v_i \frac{h}{2\pi k_{\mathrm{B}}} \sqrt[3]{6\pi^2 n}. \tag{6}$$

As can be clearly seen in Fig. 5, the diamond has the largest minimum thermal conductivity coefficient with a value of 1.13 W/(K cm). In Fig. 5, tri-$Si_{18}$ exhibits the minimum thermal conductivity of 1.10 W/(K cm), making it marginally less than that of diamond. In addition, the minimum thermal conductivity of tri-$Si_{18}$ is higher compared to that of the materials ($C2/m$-20, $C2/m$-16, $I$-4, $Pm$-3$m$, $Si_{64}$). Since the minimum thermal conductivity of tri-$Si_{18}$ is close to that of diamond-Si, tri-$Si_{18}$ possesses excellent thermal conductivity and has the potential to significantly contribute to the research of thermal insulation materials.

TABLE IV

Estimated shear wave velocity ($v_s$), compressional wave velocity ($v_p$), average sound velocity ($v_m$), and Debye temperature $\Theta_{\mathrm{D}}$ for tri-$Si_{18}$, $Amm2$, $C2/m$-20, and $Fd$-3$m$.

| | $v_p$ [m/s] | $v_s$ [m/s] | $v_m$ [m/s] | $\Theta_{\mathrm{D}}$ [K] |
|---|---|---|---|---|
| tri-$Si_{18}$ | 8640 | 5190 | 5740 | 621 |
| $Amm2$ Si[a] | 8182 | 4836 | 5357 | 575 |
| $C2/m$-20 Si[a] | 8382 | 4972 | 5506 | 595 |
| $Fd$-3$m$ Si[b] | 8727 | 5303 | 5859 | 639 |

[a]Ref [55]; [b]Ref. [56].

To further study the properties of the material, Debye temperature ($\Theta_{\mathrm{D}}$) [53, 54] is also an important parameter. The elastic Debye temperature $\Theta_{\mathrm{D}}$ and the average sound velocity $v_m$ are intimately connected, with their relationship expressed as follows

$$\Theta_{\mathrm{D}} = v_m \frac{h}{k_{\mathrm{B}}} \sqrt[3]{\left(\frac{3n}{4\pi}\right)\frac{N_A\rho}{M}}, \tag{7}$$

where $k_{\mathrm{B}}$ stands for Boltzmann's constant, $h$ stands for Planck's constant, $n$ stands for the number of atoms in the molecule, $N_A$ stands for the Avogadro number, $\rho$ stands for the density, and $M$ stands for the molecular weight. In addition,

$$v_m = \left[\frac{1}{3}\left(\frac{2}{v_s^3} + \frac{1}{v_p^3}\right)\right]^{-1/3}. \tag{8}$$

Shear wave velocity ($v_s$) and compression wave velocity ($v_p$) are estimated by Navier's equations, i.e., $v_s = (G/\rho)^{1/2}$ and $v_p = [(B + \frac{4}{3}G)/\rho]^{1/2}$.

Under normal circumstances, the bonding force between atoms is strengthened as the Debye temperature increases. Table IV (see [40, 55]) shows the estimated shear wave velocity ($v_s$), compression wave velocity ($v_p$), average sound velocity ($v_m$), and Debye temperature $\Theta_{\mathrm{D}}$ of tri-$Si_{18}$. It is noteworthy that the Debye temperature of tri-$Si_{18}$ is slightly lower than diamond-Si, as evident from the table. Also, the Debye temperature of tri-$Si_{18}$ (621 K) surpasses the values of $Amm2$ (575 K) and $C2/m$ (595 K). As a result, the stability of tri-$Si_{18}$ is better than that of $Amm2$ and $C2/m$ and falls slightly below the stability of diamond-Si.

## 4. Conclusions

Utilizing the first-principles calculation on the basis of density functional theory, we present a new silicon allotrope material featuring an indirect band gap. Furthermore, this manuscript investigated the properties of tri-$Si_{18}$ at zero pressure by

using MedeA-VASP, including structural, stability, electronic, mechanical, and anisotropic properties and the minimum thermal conductivity. Through the study of elastic constant and phonon spectrum, it can be found that tri-$Si_{18}$ is mechanically stable and dynamically stable. Through studying the elastic properties of tri-$Si_{18}$, it can be concluded it has decent brittleness. In addition, the study of the ratio of the maximum and minimum values of Young's modulus ($E$) of tri-$Si_{18}$ shows that tri-$Si_{18}$ has the largest anisotropy in the [100], [010], [110], and [111] directions. Tri-$Si_{18}$ is a semiconductor material with an indirect band gap of 1.770 eV. Furthermore, tri-$Si_{18}$ possesses a minimum thermal conductivity of 1.10 W/(K cm), which is marginally smaller compared to diamond. In addition, tri-$Si_{18}$ exhibits a higher minimum thermal conductivity compared to the other materials ($C2/m$-20, $C2/m$-16, $I$-4, $Pm$-$3m$, $Si_{64}$). This novel semiconductor silicon material (tri-$Si_{18}$) may have great potential in the manufacturing process of semiconductor devices and integrated circuits.

## References


[1] B. Haberl, T. Strobel, J. Bradby, *Appl. Phys. Rev.* **3**, 040808 (2016).

[2] Z. Naveh, R. Taghavimendi, M. Sarmazdeh, A. Bakhshayeshi, *Solid. State. Commun.* **332**, 114325 (2021).

[3] A. Oreshonkov, E. Roginskii, V. Atuchin, *J Phys. Chem. Solids.* **137**, 109219 (2020).

[4] Q. Fan, H. Peng, W. Zhang, X. Yu, S. Yun, *J. Solid. State Chem.* **305**, 122641 (2022).

[5] Q. Wang, B. Xu, J. Sun, H. Liu, Z. Zhao, D. Yu, C. Fan, J. He, *J. Am. Chem. Soc.* **136**, 9826 (2014).

[6] C. Bai, C. Chai, Q. Fan, Y. Liu, Y. Yang, *Materials* **10**, 441 (2017).

[7] X. Hao, H. Cui, *J. Korean. Phys. Soc.* **65**, 45 (2014).

[8] W. Zhang, C. Chai, Q. Fan, Y. Song, Y. Yang, *Results Phys.* **18**, 103271 (2020).

[9] L. Jantke, S. Stegmaier, A. Karttunen, T. Fässler, *Chem. Eur. J.* **23**, 2734 (2017).

[10] M. Zwijnenburg, K. Jelfs, S. Bromley, *Phys. Chem. Chem. Phys.* **12**, 8505 (2010).

[11] Y. Zhang, S. Chen, H. Xiang, X. Gong, *Carbon.* **109**, 246 (2016).

[12] D. Kim, S. Stefanoski, O. Kurakevych, T. Strobel, *Nat. Mater.* **14**, 169 (2014).

[13] Y. Guo, Q. Wang, Y. Kawazoe, P. Jena, *APS Meet.* **5**, 14342 (2015).

[14] Q. Fan, C. Chai, Q. Wei, Y. Yang, *Phys. Chem. Chem. Phys.* **18**, 12905 (2016).

[15] M. Amsler, S. Botti, M. Marques, T. Lenosky, S. Goedecker, *Phys. Rev. B* **92**, 014101 (2015).

[16] X. Shi, C. He, C. Pickard, C. Tang, J. Zhong, *Phys. Rev. B* **97**, 014104 (2018).

[17] C. He, X. Shi, S. Clark, J. Li, C. Pickard, T. Ouyang, C. Zhang, C. Tang, J. Zhong, *Phys. Rev. Lett.* **121**, 175701 (2018).

[18] Q. Fan, C. Li, R. Yang, X. Yu, W. Zhang, S. Yun, *J. Solid. State Chem.* **294**, 121894 (2021).

[19] Y. Luo, C. Ren, Y. Xu, J. Yu, S. Wang, M. Sun, *Sci. Rep.* **11**, 19008 (2021).

[20] Q. Fan, H. Liu, L. Jiang, X. Yu, W. Zhang, S. Yun, *Diam. Relat. Mater.* **116**, 108426 (2021).

[21] C. Xu, M. Zhu, J. Zhang, W. Wang, Y. Yan, *Comput. Mater. Sci.* **150**, 314 (2018).

[22] Q. Fan, H. Liu, R. Yang, X. Yu, W. Zhang, S. Yun, *J. Solid. State. Chem.* **300**, 122260 (2021).

[23] U. Arrieta, N. Katcho, O. Arcelus, J. Carrasco, *Sci. Rep.* **7**, 5350 (2017).

[24] Q. Fan, H. Liu, L. Jiang, W. Zhang, Y. Song, Q. Wei, X. Yu, S. Yun, *Nanotechnol. Rev.* **10**, 1266 (2021).

[25] P. Hohenberg, W. kohn, *Phys. Rev.* **136**, B864 (1964).

[26] W. Kohn, L. Sham, *Phys. Rev.* **140**, 133 (1965).

[27] G. Kresse, J. Furthmuller, *Phys. Rev. B* **54**, 11169 (1996).

[28] G. Kresse, J. Furthmuller, *Comput. Mater. Sci.* **6**, 15 (1996).

[29] J. Perdew, K. Burke, M. Ernzerhof, *Phys. Rev. Lett.* **77**, 3865 (1996).

[30] D. Vanderbilt, *Phys. Rev. B* **41**, 7892 (1990).

[31] B. Pfrommer, M. Côté, S. Louie, M. Cohen, *J. Comput. Phys.* **131**, 233 (1997).

[32] H. Monkhorst, J. Pack, *Phys. Rev. B* **13**, 5188 (1976).

[33] R. Hill, *Proc. Soc. A* **65**, 349 (1952).

[34] A. Krukau, O. Vydrov, A. Izmaylov, G. Scuseria, *J. Chem. Phys.* **125**, 224106 (2006).

[35] J. Heyd, G. Scuseria, M. Ernzerhof, *J. Chem. Phys.* **118**, 8207 (2003).

[36] S. Baroni, S. Gironcoli, A. Dal Corso, P. Giannozzi, *Rev. Mod. Phys.* **73**, 515 (2001).

[37] Q. Fan, R. Niu, W. Zhang, Y. Ding, S. Yun, *Chem. Phys. Chem.* **20**, 128 (2019).

[38] F. Wu, D. Jun, E. Kan, Z. Li, *Solid State Commun.* **151**, 1228 (2011).

[39] J. Hall, *Phys. Rev.* **161**, 756 (1967).

[40] Q. Fan, C. Chai, Q. Wei, H. Yan, Y. Zhao, Y. Yang, X. Yu, Y. Liu, M. Xing, J. Zhang, R. Yao, *J. Appl. Phys.* **118**, 185704 (2015).

[41] Y. Zhao, S. Lin, Q. Fan, Q. Zhang, *J. Chem. Phys.* **33**, 1 (2020).

[42] J. Wortman, R. Evans, *J. Appl. Phys.* **36**, 153 (1965).

[43] F. Mouhat, F. Coudert, *Phys. Rev. B* **90**, 224104 (2014).

[44] C. He, C. Zhang, J. Li, X. Peng, L. Meng, Chao Tang, J. Zhong, *Phys. Chem. Chem. Phys.* **18**, 9682 (2016).

[45] A. Reuss, *J. Appl. Math. Mech.* **9**, 49 (1929).

[46] R. Hill, *Phys. Soc. Lond. Sect. A* **65**, 349 (1952).

[47] Y. Ding, M. Chen, X. Gao, M. Jiang, *Chin. Phys. B* **21**, 067101 (2012).

[48] J. Watt, L. Peselnick, *J. Appl. Phys.* **51**, 1525 (1980).

[49] T. Ting, *J. Elasticity* **81**, 271 (2005).

[50] N. Korozlu, K. Colakoglu, E. Deligoz, S. Aydin, *J. Alloys Compd.* **546**, 157 (2013).

[51] D. Clarke, *Surf. Coat. Technol.* **163**, 67 (2003).

[52] D. Cahill, S. Watson, R. Pohl, *Phys. Rev. B* **46**, 6131 (1992).

[53] Q. Fan, Q. Wei, C. Chai, M. Zhang, H. Yan, Z. Zhang, J. Zhang, D. Zhang, *Comput. Mater. Sci.* **97**, 6 (2014).

[54] O. Anderson, *J. Phys. Chem. Solids* **24**, 909 (1963).

[55] Y. Zhao, W. Zhang, Q. Fan, *Commun. Theor. Phys.* **71**, 1036 (2019).